Inter J Nav Archit Oc Engng (2009) 1:101~107
DOI 10.3744/JNAOE.2009.1.2.101

Cross flow response of a cylindrical structure under local shear flow

Yoo-Chul Kim[1,2] and Chang-Kyu Rheem[1]

[1]*Institute of Industrial Science, the University of Tokyo, Tokyo, JAPAN*
[2]*Research Institute of Marine Systems Engineering, Seoul National University, Seoul, Korea*

ABSTRACT: *The VIV (Vortex-Induced Vibration) analysis of a flexible cylindrical structure under locally strong shear flow is presented. The model is made of Teflon and has 9.5m length, 0.0127m diameter, and 0.001m wall thickness. 11 2-dimensional accelerometers are installed along the model. The experiment has been conducted at the ocean engineering basin in the University of Tokyo in which uniform current can be generated. The model is installed at about 30 degree of slope and submerged by almost overall length. Local shear flow is made by superposing uniform current and accelerated flow generated by an impeller. The results of frequency and modal analysis are presented.*

KEY WORDS: Ocean Risers; VIV (Vortex-Induced Vibration); Flexible Cylinder.

INTRODUCTION

When a cylindrical structure is placed in a current, the vortices are generated by viscosity at both sides of the cylinder and finally shed from the wall. The vortices are developed symmetrically at first but the symmetry breaks soon, which generates alternatively shedding vortices called Karman vortex street. These vortices induce forces to the structure according to relative location and cause the periodic vibration known as vortex-induced vibration (VIV). VIV is often observed at chimneys, electric wires, offshore structures, etc. and has recently emerged as one of the crucial problems in ocean risers. Ocean risers are relatively flexible structures due to high aspect ratio (length to diameter), which gives rise to high mode vibrations. In addition, various inflows along the structure make the behavior more complicated. These characteristics make it difficult to design risers and demand accurate prediction of VIV responses.

A lot of elaborate researches for VIV responses of cylindrical structures have been conducted for some decades. *Comprehensive reviews* for VIV have been presented by Sarpkaya (2004), Griffin and Ramberg (1974), Bearman (1984), Parkinson (1989), Sumer and Fredsoe (1997), etc. *For rigid cylinders*, flow visualization for forced oscillation using Aluminum particles was conducted by Williamson and Roshko (1988). Govardhan and Williamson (2000) have introduced vortex force and total force to explain change of vortex formation in case of free oscillating cylinder. The free and forced oscillation of uniform and tapered cylinder and inline and transverse vibration of a rigid cylinder have been studied by Hover et al. (1998) and Sanchis et al. (2008), respectively. Cylinder response according to inline versus transverse frequency ratio has also presented by Dahl et al. (2006). *For flexible cylinders* which are more practical for applying to ocean risers, Fujarra et al. (2001) have compared response characteristics of flexible cantilever cylinder and elastically mounted rigid cylinder. Lie and Kaasen (2006) have conducted large scale model test of tensioned steel riser. Model test of bare and straked riser with high aspect ratio and vertical riser test under step flow have been conducted by Trim et al. (2005) and Chaplin et al. (2005), respectively.

Although past researches have mainly focused on responses of cylinder under uniform or linear shear flow, real sea state in which ocean risers are installed might be more complicated. In this viewpoint, locally strong shear flow might be considered as more realistic, therefore VIV characteristics of a flexible cylindrical structure under local shear flow are presented in this paper. The details of experimental setup and measured inflows are presented in Section 2 and Section 3, respectively. The results of VIV response are shown in Section 4. Some discussions are drawn in Section 5.

Corresponding author: *Chang-Kyu Rheem*
e-mail: *rheem@iis.u-tokyo.ac.jp*

EXPERIMENTAL SETUP

The experiment has been conducted at the ocean engineering basin in the University of Tokyo whose width is 10*m*, depth is 5*m*, and length is 50*m*. The overall length of the riser model is 9.5*m* and the cross section has 0.0127*m* diameter and wall thickness of 0.001*m*, and water is filled in the model during experiment. The details of the model are shown in Table 1. The lower end of the model is fixed on the bottom of the basin with universal joint and the other end is connected to some weights out the water to apply top tension.

Table 1 Riser model properties.

Length	9.5*m*
Diameter	0.0127*m*
Wall Thickness	0.001 *m*
Material	Teflon
Specific Gravity	2.2
End Condition	Universal Joint

The model is installed with leaning pose by about 30 degree to be submerged in the water as shown in Fig. 1. Inline and transverse motions are measured at 11 accelerometers set up along the model.

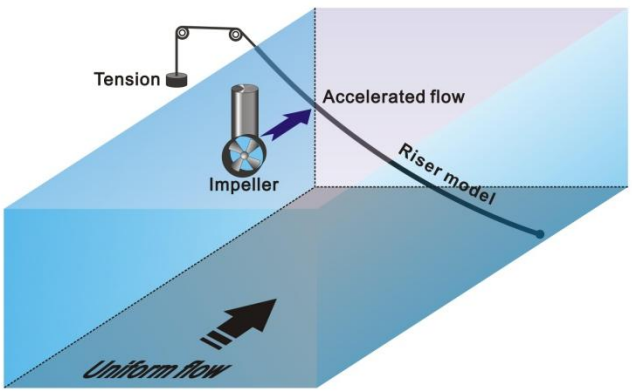

Fig. 1 Overview sketch of experimental setup.

First five accelerometers are placed with 1*m* interval started at 1m off the bottom and the rest with 0.5*m* interval as illustrated in Fig. 2. The numbering starts from the top one to the bottom one.

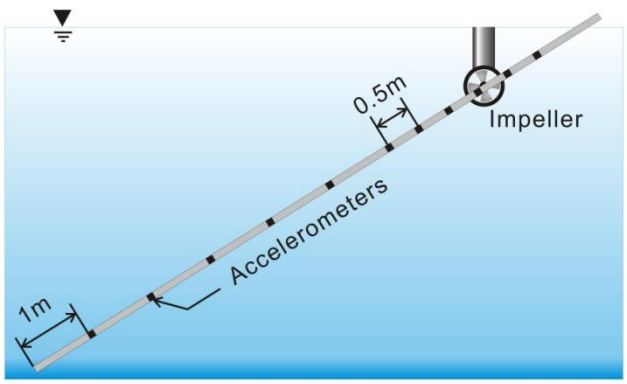

Fig. 2 Location of accelerometers and the impeller.

In order to generate local shear profile, a current generator (denoted by *f* in Fig. 3) equipped in the basin and a pod type impeller is used. Specifically, narrow and fast flow accelerated by the impeller is superposed on uniform current made by the current generator. The center of the impeller with 0.3*m* diameter is located under water surface by 0.72 *m* which is in between 2nd and 3rd accelerometer as shown in Fig. 2, and upstream by about 1.5 *m* from the riser model. Fig. 4 indicates the installed riser model.

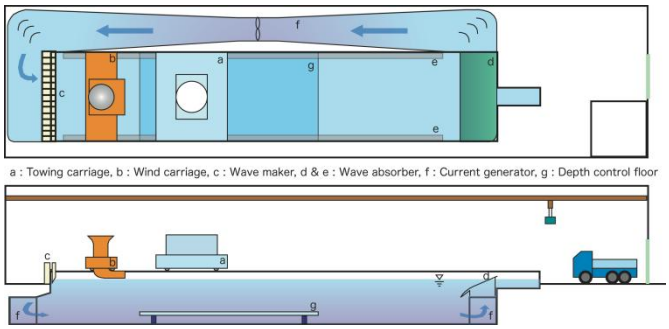

Fig. 3 Layout of the ocean engineering basin.

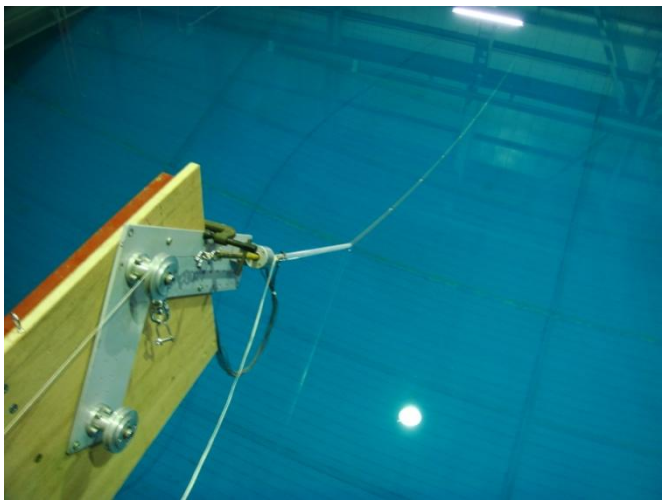

Fig. 4 The installed riser model.

VELOCITY PROFILES

Measuring velocity component incoming to the riser model is needed since inflow is generated by controlling not the model but the flow. Velocities are measured for 8 flow conditions in which 3 uniform currents (U=0, 0.05, 0.1*m/s*) and 3 local flows (L=0, 0.2, 0.4*m/s*) are included and interpolation scheme is used for other flow conditions. Although the best way to get the inflow information is to measure the velocity on the spot at which accelerometers are located, we have measured velocities at some points near the impeller in which velocity gradient is somewhat high due to a given experimental condition. We assumed that the velocity distribution is axisymmetric around rotation axis of the impeller, which means that depth-wise velocity profile can be expanded along the model. Inflow velocities are measured at depth-wise 8 points from the center of the impeller as shown

in Fig. 5 and velocities at more distant points than the 8th measuring point are considered as uniform current.

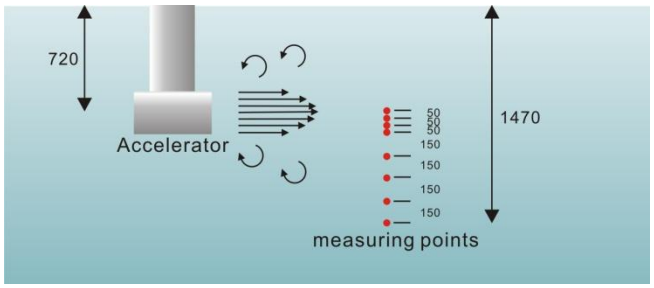

Fig. 5 Measuring points for inflow velocity.

Fig. 6 indicates velocity profiles measured under only uniform currents. Velocities around the center of the impeller are lower than those of distant points because the measuring points corresponding to location of the model are behind the impeller. Uniform velocity profile is obtained except near the center.

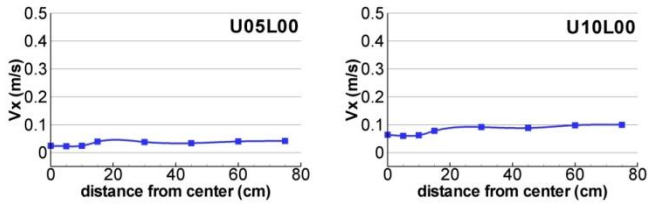

Fig. 6 Velocity profiles of uniform flow.

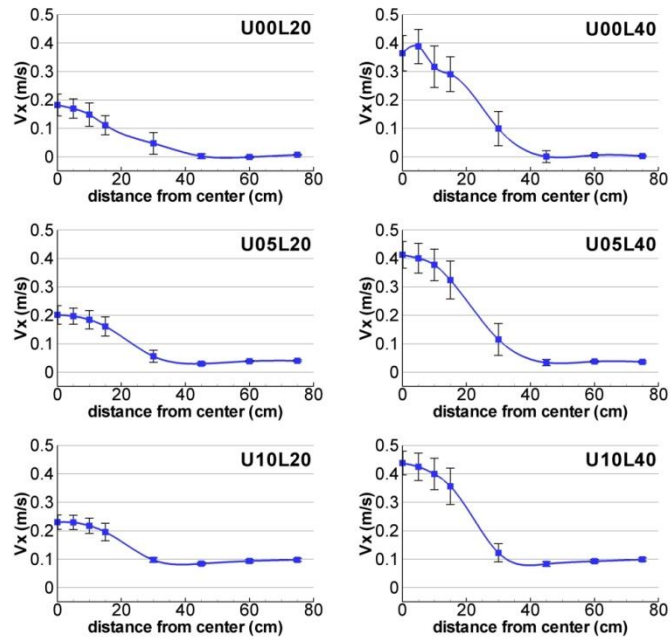

Fig. 7 Velocity profiles of shear flows

Fig. 7 provides the measured velocity profiles under local shear flow. Velocity near the center is high as expected and that of distant point is almost same as the uniform current. Fig. 7 in which standard deviation of velocity is shown makes it confirmed that the flow around the impeller is rather unstable because of strong wake. The deviation is about 10 percent of the averaged value except around the impeller radius. The averaged velocities for U05 and U10 are 0.04*1m*/s and 0.099*m/s*, respectively. Figures indicate that the influence of the impeller disappears if it is far from the center by about twice the impeller's diameter.

VIV RESPONSES

We use the following approach to convert acceleration obtained from each accelerometer into displacement. FFT (fast Fourier transform) and band-pass filter are applied in order to obtain noise-filtered frequency component. Low frequency for the filter is adopted as half the lower value of the 1st natural frequency of the model and Strouhal frequency (f_S) corresponding to the maximum local velocity and twice the higher value is applied for the low-pass filter. Filtered time series of vibration displacement are obtained by dividing acceleration by angular velocity ($-\omega^2$) corresponding to each frequency and then applying inverse Fourier transform under assumption that vibration of the model is periodic. Strouhal frequency is calculated assuming Strouhal number is 0.2 and natural frequency of the model is done using tensioned beam theory (Timoshenko et al., 1974). Hence ith natural frequency (f_{ni}) is given as:

$$f_{n_{string}} = \frac{n}{2}\sqrt{\frac{T}{mL^2}}$$
$$f_{n_{beam}} = \frac{\pi n^2}{2}\sqrt{\frac{EI}{mL^4}} \quad (1)$$
$$f_{ni} = \sqrt{f_{n_{string}}^2 + f_{n_{beam}}^2}$$

where n is mode number, T is top tension, m is sectional mass, E is Young's modulus and I is 2nd moment of area. It is noted that the added mass coefficient is explicitly applied as 1.0 calculating overall mass and the prescribed top tension is used. The calculated natural frequency is corrected to be correspondent to measured value through pluck test. In this study, correction parameter is 0.95. Four experiments have been conducted in this study. The first one is preliminary test for general characteristics under local shear flow. In the second experiment, uniform flow case in which base current increases from 0.04*m/s* to 0.13*m/s* is tested. Two local flows for five base currents are applied for the third experiment and increasing local flow with small step is applied as well. Top tensions of 4 *kgf* and 6*kgf* are applied except for the first test.

Experiment I (preliminary test)

Three base currents and local flows are applied for this preliminary test. Under 4 top tensions (2, 4, 6, 8*kgf*), we set up the base current (U) as 0, 0.05, 0.1*m*/s and local flow (L) as 0, 0.2, 0.4*m/s* which are corresponding to impeller's rps 0, 5, 10.

The power spectral densities (PSD) of cross flow displacements for U10 are shown in Fig. 8.

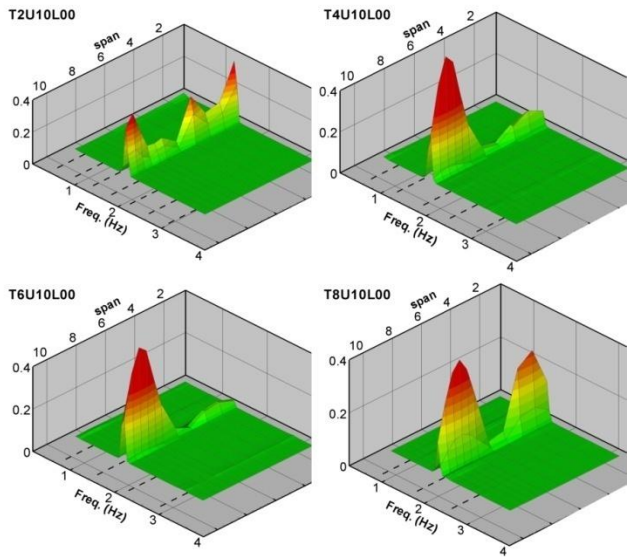

Fig. 8 PSD of cross flow displacement at each top tension.

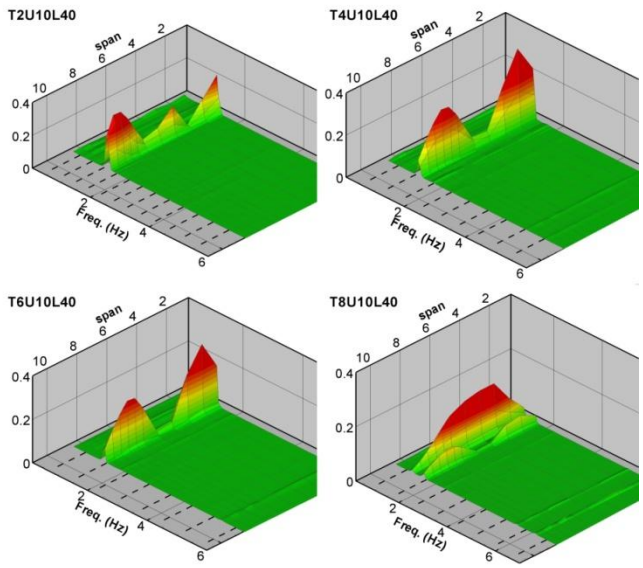

Fig. 9 PSD of cross flow displacement under local shear flow.

The dashed line indicates natural frequency in static water. The peak appears around f_{n3} at T2 and f_{n2} at the others since the natural frequency necessarily decreases with increasing top tension as Eq. 1. It is confirmed that the shape of PSD is determined by the correlation between natural frequency and peak frequency from the fact that three peaks along the span are shown at T2 and two peaks are shown at the others. Different peak amplitude along the span might be caused from end condition of the model of which top end is not fixed completely but free to slide along the axis. Fig. 9 shows cross flow PSD under local shear flow (U10L40). The main peak frequency seldom changes even adopting local shear flow except T8, which will be discussed later in 4.3. However, vibration components caused from local flow appear near the peak frequency and at high frequency around 6*Hz* even though they have relatively small amplitude. It is also confirmed that intermediate frequency components between peak frequency and the high frequency have very small amplitude as shown in Fig. 9, which will be discussed in 4.4.

Experiment II (uniform flow)

The measurement has been conducted changing base current from 0.04*m/s* to 0.13*m/s* by 0.01*m/s* interval for 4 and 6 *kgf* top tensions. Fig. 10 shows frequency ratio of peak frequency to the 1st natural frequency.

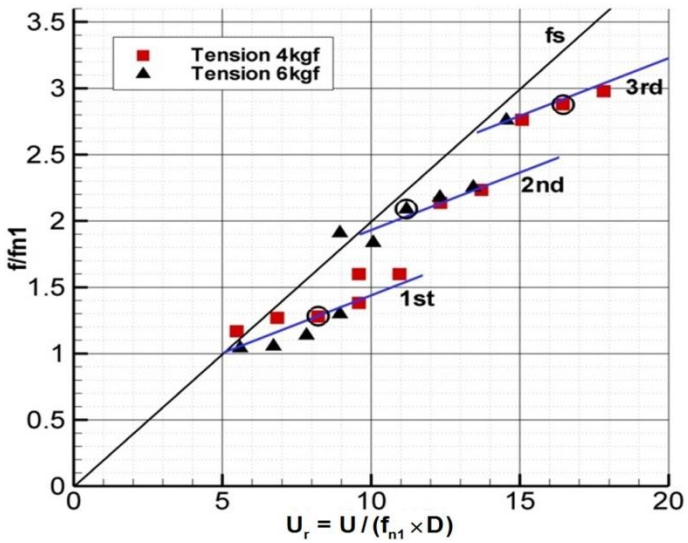

Fig. 10 Peak frequency ratio under uniform flow.

The condition that U = 0.04*m/s* for 6*kgf* top tension is excluded from the plot because of too much small response. Frequency jumps can be seen around Ur =10 and 15 and then the ratio increases with the lower slope than that of Strouhal frequency that is vortex shedding frequency for a fixed cylinder (assumed as 0.2 in this plot). This phenomenon means that vortex shedding frequency and structural vibrating frequency are synchronized, which is called as lock-in. It is generally verified that further increase of Ur after synchronization of Strouhal frequency and natural frequency pulls the shedding frequency away from its nonoscillating value for a rigid cylinder with low mass ratio (Khalak and Williamson, 1999).

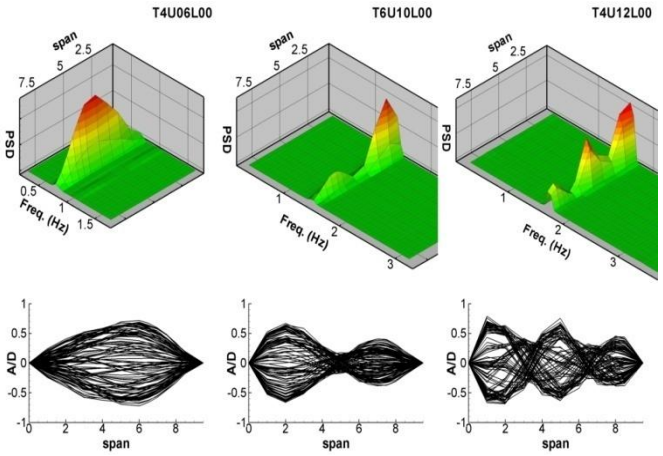

Fig. 11 PSD and mode shapes.

It is confirmed that similar trend appears in a flexible cylinder. Fig. 11 indicate PSD and accumulated time-series of displacement for the cases of T4U06L00, T6U10L00, and T4U12L00, respectively (denoted by circles in Fig. 10). Each condition corresponds to Ur=8, 11, 16. The vibration mode of the structure is determined according to its synchronization region. Specifically, the structure shows the 1st mode vibration before Ur=10 and then vibration mode changes to the 2nd mode after that. Two peaks of PSD appear near the frequency jump (Ur=10) in Fig. 10, which is caused by instability between two vibration modes.

Experiment III (local shear flow)

Four base currents are selected and 4 and 7 times faster local flows than each base current are adopted. The selected base currents are 0.03, 0.05, 0.07, 0.09, and 0.11 *m/s*. Fig. 12 shows projected PSD at each accelerometer on the frequency-PSD plane under the condition that base current is in the synchronization regime. Local shear flow is applied only for 2nd and 3rd rows of Fig. 12.

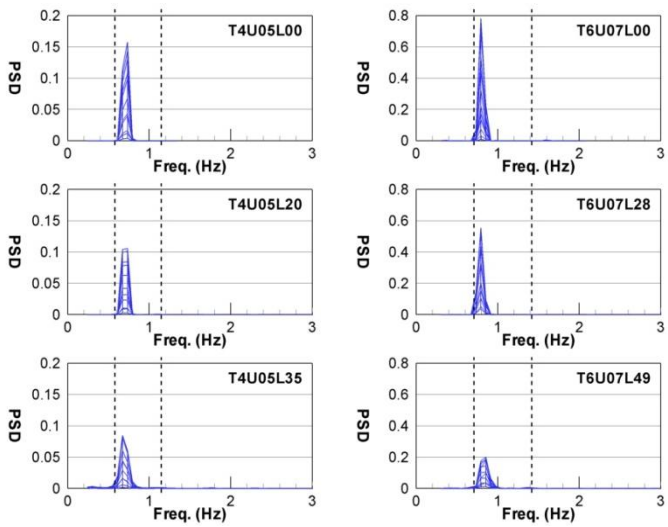

Fig. 12 Change of vibration energy according to local flow in the synchronization regime.

The dashed lines indicate natural frequencies. There is no change in peak frequency even though local flow increases. However, it is confirmed that amplitude of PSD which can be thought as vibration energy goes down with increasing local flow intensity. This is reasonable since inflow which induces synchronized vibration is disturbed by local flow and this local flow contributes higher frequency components. It means that local flow disperses lock-in vibration and results in decreasing vibration energy. Fig. 13 shows PSDs under the condition that base currents are around the region in which vibration mode changes. The peak frequency under only base current moves to the direction of lower frequency as local flow increases and two peaks are shown as well (see the second row of the plot). Precisely in the right side of Fig. 13, there is a peak near 1.3*Hz* at first, but another peak around 1*Hz* occurs and it becomes dominant finally. This means that there are two vibration modes competing near where mode changes, and once the input energy exceeds any threshold, the vibration governed by Strouhal frequency becomes dominant. In other words, input energy level for maintaining lock-in vibration is lower than that for Strouhal vibration.

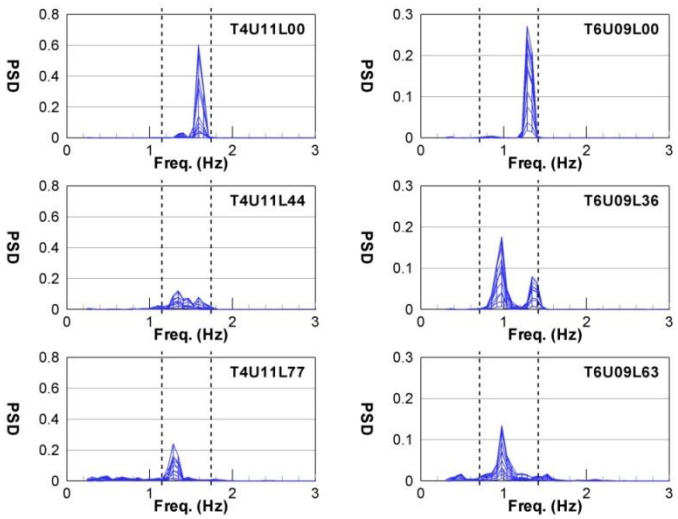

Fig. 13 Change of peak frequency according to local flow in the region where mode changes.

Experiment IV (increasing local flow)

We have focused on frequency components increasing local flow velocity in order to see relationship between local velocity and vibration mode in this test. We have setup the base current as 0.07 and 0.08 *m/s* respectively for 4 and 6 *kgf* top tensions and local flow from 0.04 *m/s* to 0.4 *m/s* with 0.02 *m/s* interval. Fig. 14 shows PSD in log-scale manner with respect to each local flow velocity for 4*kgf* top tension. There is no change in dominant peak frequency and high frequency components come to be shown as local flow velocity is getting higher. It is also confirmed that peak frequencies according to local flow are shown around natural frequencies indicated by dashed lines. The vibration energy

does not decrease in sequential order of mode number from the maximum peak in the case of T4U07L38. Precisely, 7th, 8th and 9th components are higher than 5th and 6th components.

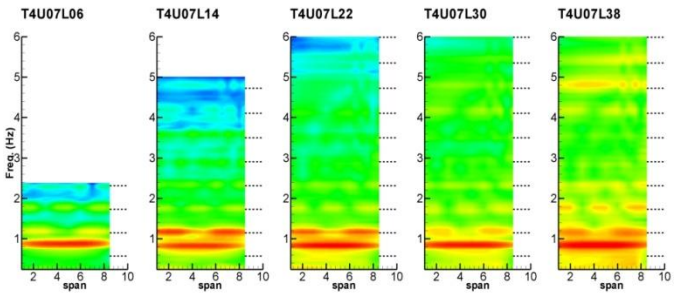

Fig. 14 Change of PSD contour as local flow increases.

Fig. 15 shows a pictogram of a velocity profile. If we assume that ith vibration mode starts at the inflow velocity at which reduced velocity corresponding to ith natural frequency is 5, we can calculate the structural length (hereafter mode length) corresponding to ith vibration mode from the inflow profile as shown in Fig. 15.

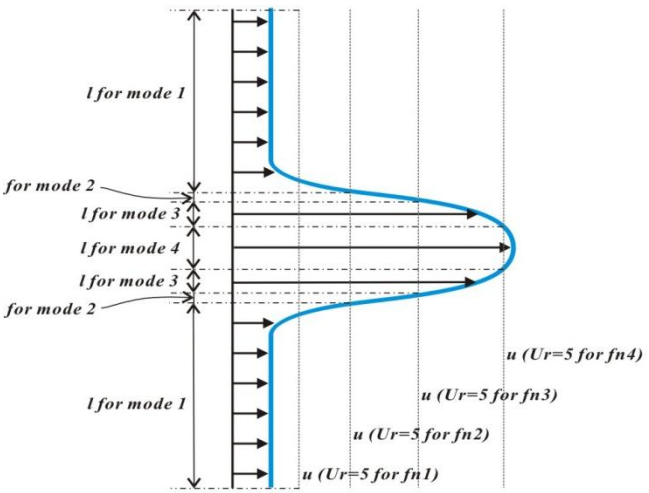

Fig. 15 Definition of mode length.

The upper figure of Fig. 16 shows log-scaled mode length for T4U05L40 and the lower one indicates measured log-scaled PSD for the same condition. Both graphs show the peak at the 8th mode except the 1st mode induced by the base current. This result hints that there is a strong correlation between mode length and vibration energy under local shear flow. However, the 2nd, 3rd and 4th modes have very low value at mode length plot although they show somewhat high value at PSD plot. This result might be caused from instability of inflow especially around where inflow velocity increases from the base current due to vortical flow.

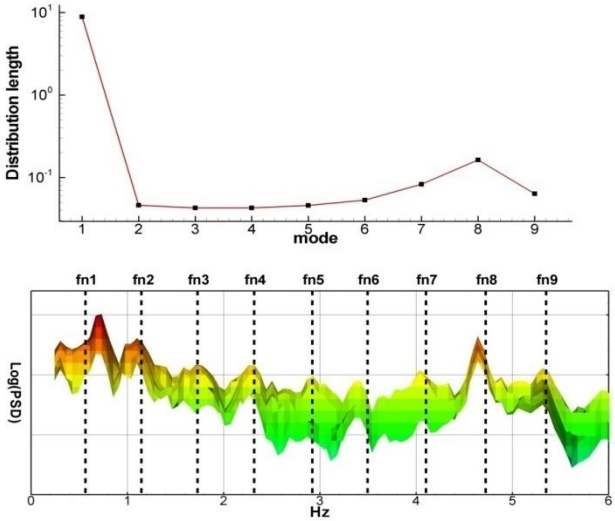

Fig. 16 Comparison of mode length and PSD distribution.

CONCLUDING REMARKS

Cross flow VIV responses under local shear flow have been investigated in this study. In uniform flow experiment, common VIV characteristics are verified such as lock-in phenomenon. Once VIV enters lock-in regime, added mass changes and vibration frequency is regulated by not Strouhal frequency but natural frequency. This synchronization continues until one vibration mode progresses the next one. Under local shear flows, the dominant vibration mode is determined by base current and some other frequency components appear at high frequency. However, local shear flow influences vibration energy level and peak frequency at some conditions. Vibration energy in the lock-in regime decreases under strong local shear flow and peak frequency becomes lower around the region where vibration mode changes, which hint that local disturbance makes the lock-in vibration energy dispersed and the energy level for lock-in vibration is much lower than that for Strouhal vibration. We have also derived that the amplitude of each vibration mode has strong correlation with shear profile of inflow.

Our future plans consist in more detailed control of base current and shear flow velocity and location of shear profile along the riser model.

REFERENCES

Bearman, P.W., 1984. Vortex shedding from oscillating bluff bodies. *Annual Reviews of Fluid Mechanics*, 16, pp. 195-222.

Chaplin, J.R. Bearman, P.W. Huera Huarte, F.J. Pattenden, R.J., 2005. Laboratory measurements of vortex-induced vibrations of a vertical tension riser in a stepped current. *J. Fluids Struct.*, 21, pp. 3-24.

Dahl, J.M. Hover, F.S. Triantafyllou, M.S., 2006. Two-degree-of-freedom vortex-induced vibrations using a force assisted apparatus. *J. Fluids Struct.*, 22, pp. 807-818.

Fujarra, A.L.C. Pesce, C.P. Flemming, F. Williamson, C.H.K., 2001. Vortex-induced vibration of a flexible cantilever. *J. Fluids Struct.*, 15, pp. 651-658.

Griffin, O.M. Ramberg, S.E., 1974. The vortex-street wakes of vibrating cylinders. *J. Fluid Mech.*, 66, pp. 553-576.

Govardhan, R. and Williamson, C.H.K., 2000. Modes of vortex formation and frequency response of a freely vibrating cylinder. *J. Fluid Mech.*, 410, pp. 85-130.

Hover, F.S. Techet, A.H. Triantafyllou, M.S., 1998. Forces on oscillating uniform and tapered cylinders in crossflow. *J. Fluid Mech.*, 363, pp. 97-114.

Khalak, A. Williamson, C.H.K., 1999. Motions, forces and mode transitions in vortex-induced vibrations at low mass-damping. *J. Fluids Struct.*, 13, pp. 813-851.

Lie, H. Kaasen, K.E., 2006. Modal analysis of measurements from a large-scale VIV model test of a riser in linearly sheared flow. *J. Fluids Struct.*, 22, pp. 557-575.

Parkinson, G., 1989. Phenomena and modelling of flow-induced vibration of bluff bodies. *Progress in Aerospace Science*, 26, pp. 169-224.

Sanchis, A. Salevik, G. Grue, J., 2008. Two-degree-of-freedom vortex-induced vibrations of a spring-mounted rigid cylinder with low mass ratio. *J. Fluids Struct.*, 24, pp. 907-919.

Sarpkaya, T., 2004, A critical review of the intrinsic nature of vortex-indeuced vibrations. *J. Fluids Struct.*, 19, pp. 389-447.

Sumer, B.T. and Fredsoe, J., 1997, *Hydrodynamics around cylindrical structures*, World Scientific publishing, Lodon

Timoshenko et al., 1974. *Vibration problems in engineering*. 4th ed. New York, USA: John Wiley and Sons.

Trim, A.D. Braaten, H. Lie, H. Tognarelli, M.A., 2005. Experimental investigation of vortex-induced vibration of long marine risers. *J. Fluids Struct.*, 21, pp. 335-361.

Williamson, C.H.K. and Roshko, A., 1988. Vortex formation in the wake of an oscillating cylinder. *J. Fluids Struct.*, 2, pp. 355-381.